A Reliability Model for Integrated Energy System Considering Multi-energy Correlation

Chao Yan, Zhaohong Bie, Shiyu Liu, Dogan Urgun, Chanan Singh, and Le Xie

Abstract—An integrated energy system (IES) is a regional energy system incorporating distributed multi-energy systems to serve various energy demands such as electricity, heating, cooling, and gas. The reliability analysis plays a key role in guaranteeing the safety and adequacy of an IES. This paper aims to build a capacity reliability model of an IES. The multi-energy correlation in the IES can generate the dependent capacity outage states, which is the distinguished reliability feature of an IES from a generation system. To address this issue, this paper presents a novel analytical method to model the dependent multi-energy capacity outage states and their joint outage probabilities of an IES for its reliability assessment. To model the dependent multi-energy capacity outage states, a new multi-dimensional matrix method is presented in the capacity outage probability table (COPT) model of the generation system. Furthermore, a customized multi-dimensional discrete convolution algorithm is proposed to compute the reliability model, and the adequacy indices are calculated in an accurate and efficient way. Case studies demonstrate the correctness and efficiency of the proposed method. The capacity value of multi-energy conversion facilities is also quantified by the proposed method.

Index Terms—Capacity outage probability table (COPT), integrated energy system (IES), multi-dimensional discrete convolution, reliability model.

I. INTRODUCTION

N recent years, the integrated energy system (IES) is gaining widespread application around the world [1], [2]. An IES emphasizes the complementarity and synergy of various forms of energy such as electricity, heating, cooling, and gas. It enhances the operation efficiency of the whole energy system, integrates more distributed renewable energy resources and improves the adequacy of different forms of energy supplies [3], [4]. Also, it enables closer correlations among

DOI: 10.35833/MPCE.2020.000301

multi-energy systems by the coupling of multi-energy systems.

In general, the components in the IES, i.e., the multi-energy generation (MEG) facilities or the multi-energy conversion (MEC) facilities, are coupled with various energy systems with certain correlations. This motivates wide studies on an IES from different aspects. For example, [5]-[7] study the calculations of energy flow, probabilistic energy flow, and optimal energy flow of an IES. An optimal operation and management strategy for an IES is proposed in [8], [9]. And the optimal expansion planning and design of an IES are studied in [10], [11].

The reliability evaluation of an IES with the corresponding metrics such as adequacy and capacity values is also an important aspect that requires deep research. References [12], [13] construct an analytical reliability model of a multi-energy system for its supply reliability considering the conversion of different energy forms based on Markov state space. Reference [14] studies a sampling-based simulation method to evaluate the adequacy of an IES considering the availability of the primary resources and the load dependencies of the demand side. In [15], a hierarchical decoupling optimization framework and an impact-increment-based state enumeration method (SEM) are proposed to assess the adequacy of a large-scale IES.

Recently, there are also some researches focusing on the adequacy evaluation of an IES considering more complex network failures, operation constraints, and even renewable uncertainty. The Monte-Carlo-simulation (MCS) -based reliability evaluation methods are applied to integrated electricity-heating energy system (IEHS) [16] and integrated electricity-gas energy system (IEGS) [17], with a combined multienergy optimal power flow optimization model. Reference [18] proposes a fast analytical method to cope with the adequacy assessment of IEGS considering the dispatch strategies. References [19] and [20] develop an equivalent reliability model for natural gas network based on a state transferring technique and universal generation function (UGF), respectively. They can depict the impact of stochastic failures and operation characteristics of the natural gas network on the electricity network. Reference [21] combines the above network equivalent method and the optimal power flow simulation method. A new analytical method is proposed to estimate the failure probability of an IES considering multiple correlated failure risks based on a reliability estimation theory [22]. In addition, [23] proposes a data-driven robust ap-



Manuscript received: May 11, 2020; accepted: November 2, 2020. Date of CrossCheck: November 2, 2020. Date of online publication: February 9, 2021.

This work was supported in part by the National Natural Science Foundation of China (No. 51637008) and the National Key Research and Development Program of China (No. 2016YFB0901900).

This article is distributed under the terms of the Creative Commons Attribution 4.0 International License (http://creativecommons.org/licenses/by/4.0/).

C. Yan, Z. Bie (corresponding author) and S. Liu are with the Department of Electrical Engineering, Xi'an Jiaotong University, Xi'an 710049, China, and they are also with the State Key Laboratory of Electrical Insulation and Power Equipment, Xi'an Jiaotong University, Xi'an 710049, China (e-mail: yanchao19911224@stu.xjtu.edu.cn; zhbie@mail.xjtu.edu.cn; liushiyu982@stu.xjtu.edu.cn).

D. Urgun, C. Singh, and L. Xie are with the Department of Electrical & Computer Engineering, Texas A&M University, College Station, TX 77843, USA (e-mail: doganurgun@gmail.com; singh@ece.tamu.edu; le.xie@tamu.edu).

proach for the risk evaluation of IEHS considering the ambiguous uncertainty of probability distribution of uncertainty factors

However, the capacity adequacy of an IES system has been seldom studied. In particular, the capacity reliability model of an IES, as the basic generation capacity model in the field of power system reliability, should be developed. The capacity reliability model presents the capacity outage states and the corresponding probability distributions [24]. Different from the generation system capacity model, the model should incorporate the impact of the main feature of an IES, i.e., the multi-energy correlation, which is derived from the coupling of different energy systems. Specifically, the dependent outage and the correlation of multi-energy loads are two kinds of multi-energy correlations. They will cause dependent multi-energy capacity outage states. The common-cause outage in MEG, e.g., the outage of a CHP that may lead to the simultaneous outage of power and heating capacities, and the energy-shortage-related outage in MEC, e.g., the shortage of electricity that may lead to the power-to-heat (P2H) unavailability, are all dependent outages. Meanwhile, the correlation of different energy loads is quite common.

In this paper, a novel capacity outage probability table (COPT) of IES is proposed to model these dependent multienergy capacity outage states and depict the reliability features of IES more accurately. Also, a customized convolution algorithm is also proposed to compute the analytical model effectively. The capacity value of MEC in the IES is first studied. Reference [13] successfully constructs a matrixbased energy hub reliability model by the Markov state space method considering the availability of multi-energy conversion paths. But it lacks considerations of the simultaneous outage in the MEG facilities. In addition, for largescale systems, the state spaces of the model may be immense. Our model can avoid the immense state spaces in the large-scale systems by merging the similar capacity states in the convolution computation. Reference [20] constructs an equivalent multi-state model for natural gas network to represent the effect of the coupling of the power and natural gas systems by the UFG. The reliability model in [19] is similar. Then the impact of the natural gas system on the reliability of the power system can be analyzed effectively. However, the reliability models for different energy systems are separated. That is not a whole IES reliability model considering the impacts of multi-energy coupling. It is also unknown whether the method can be applied to IEHS or other more IESs. The model proposed in this paper represents the reliability states of the whole IES, and it is also applicable to other IESs.

Usually, the COPT is an analytical method in the generation expansion planning to calculate the generation system adequacy considering the forced outage of generations [24], [25]. By constructing the capacity outage states in a discrete convolution method, this method provides not only the adequacy indices but also the probability distribution of those capacity outage states. This method is also extended to model the stochastic output of wind energy [26], even with the

consideration of wind farm correlation, output variability, and forced outages [27], [28]. In [29], a reliability-based IES planning model considers the capacity outage of power and natural gas systems. However, these COPTs are still traditional models for the single energy system, which cannot reflect the dependent outages or the correlation of multi-energy loads in the IES. The traditional COPT model uses vectors to model the outage of the generation system, but independent vectors cannot model the dependent capacity outage states of a multi-energy system. We propose the multi-dimensional matrices to model dependent multi-energy capacity outage states and their joint outage probabilities. To maintain the computation advantage of the COPT model over the SEM by the discrete convolution method, we propose the two-dimensional (2-D) discrete convolution [30] to compute the proposed IES COPT model effectively. To make sure that the algorithm can compute the exact results considering the dependent outage and the correlation of multi-energy loads, some customized computation rules are developed into the crude 2-D discrete convolution algorithm. After convolving with the multi-energy load model, an IES reserve model is then obtained. Based on the model, the exact adequacy indices of each single energy system can be gained, while some adequacy indices are calculated to indicate the impact of the multi-energy correlation for the whole IES. In particular, a conditional probability approach is proposed to integrate the MEC into the 2-D discrete convolution algorithm. Then, based on the novel capacity reliability model of an IES, the capacity value of MEC in an IES can be computed naturally to quantify its contributions to the adequacy of an IES considering its dependency on the power system. So far, most researches on capacity value only focus on wind energy. This paper proposes a pioneer study on the capacity of energy conversion facilities in an IES. Finally, an IEHS is applied to illustrate the proposed method. The contributions of this paper are threefold as follows.

- 1) We propose an analytical capacity reliability model of an IES based on the COPT. It considers the impact of multienergy correlations by using multi-dimensional matrices to model the dependent capacity outage states and their joint outage probabilities in the COPT of IES. The dependent outage and the correlated multi-energy loads can be naturally represented by this model.
- 2) A customized 2-D discrete convolution algorithm with some special computation rules is proposed. It can calculate the proposed COPT of IES correctly and fast considering the impact of dependent outage and the correlation of multi-energy loads. Meanwhile, it also maintains the computation advantage over the SEM, as the COPT of the generation system does.
- 3) The indices of an IES and some indices representing the impacts of multi-energy correlations on the capacity adequacy can be calculated. The capacity value of the multi-energy conversion in the IES is first studied to quantify its adequacy contribution considering the multi-energy coupling.

With the development of the IES, the proposed IES capacity model has the potential to support the capacity expansion planning [10] of an IES, and also a day-ahead or on-line re-

serve check of IES [31]. The multi-state reliability model can also be used in a sampling-based simulation for a more complex energy system including multiple IESs [29].

The remainder of this paper is organized as follows. Section II presents the reliability model of an IES. Section III illustrates the computation method. Section IV validates the correctness and computation performance. Section V provides the conclusion and the future work.

II. RELIABILITY MODEL OF AN IES

The multi-energy generation (MEG) and multi-energy conversion (MEC) facilities need to be invested in an IES. The dependent outage, i. e., the common-cause outage in MEG and the energy-shortage-related outage in MEC, and the correlated multi-energy loads might affect the system reliability. In this context, this section presents a reliability model of an IES in the form of dependent capacity outage states, joint outage probability, and joint cumulative outage probability distributions, which is a COPT of IES.

The COPT model is a commonly used method to calculate the adequacy of generation system. It can also be a generation reliability model of capacity outage states for power system simulation. The details of the COPT model for the power system can be found in [24], [25].

The common-cause failure can result in a simultaneous outage of multi-energy generation outputs, while the shortage of input energy can lead to the outage of output energy in multi-energy conversion facilities. On the other hand, the multi-energy loads are also correlated. These correlations lead to dependent capacity outage states in an IES. The capacity outage states in the COPT model indicate the amount of capacity that is out of service.

In general, the schematic diagram for the generation system and IES is described in Fig. 1. The MEG, combined heat and power (CHP) production, MEC, and P2H are deployed in the system. The heat energy unit is British thermal unit (Btu), which can be converted to MW by 1 W=3.412 Btu/h.

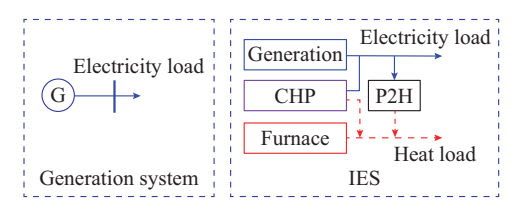


Fig. 1. Schematic diagram for generation system and IES.

A. COPT Models of Components

1) COPT Model of CHP

We first model the operation state spaces of a CHP based on a stationary discrete-time Markov process. It is assumed that the failure and repair rates of all components are constants over time, which is called time-homogeneous property. Meanwhile, in the Markov process, the next state is only related to the current state but not related to the whole history.

The operation state space for the reliability and availability of a CHP is shown in Fig. 2. The details can be found in

[32]. Three subsystems, i.e., gas, electricity, and thermal subsystems, are considered in a CHP, denoted by S_g , S_{ele} , and S_{th} , respectively. Note that these subsystems are inside a CHP, and they are different from the power or heat energy system discussed in this paper. For each subsystem, there are two operation states, i.e., normal and failed, shown by the symbols " $\sqrt{\ }$ " and " \times ", respectively.

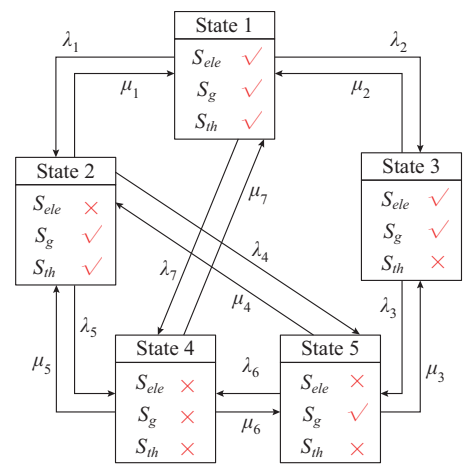


Fig. 2. Operation state space of CHP.

As the electricity and thermal subsystems are coupled with the gas subsystem, the failure in gas subsystem will cause the outage of other two subsystems together, which is called a common-cause outage. Thereby, three related states: ① {gas subsystem (failed), electricity subsystem (normal), thermal subsystem (normal)}; ② {gas subsystem (failed), electricity subsystem (failed), electricity subsystem (normal)}; ③ {gas subsystem (failed), electricity subsystem (normal), thermal subsystem (failed)} do not exist in reality. The operation state is represented by State 4 in Fig. 2, which can cause a simultaneous outage of power and heat capacities. In addition, the fuel-delivery subsystem failure is also an event of common-cause outage for the power and heat capacities. It is represented by State 5 in Fig. 2, where $\lambda_1 - \lambda_7$ and $\mu_1 - \mu_7$ are the transition rates between different system operation states.

Further, we can calculate the stationary residing probability P_i of each operation state i in Fig. 2 by the stationary probability distribution of the stationary Markov process [24]. In Fig. 2, States 4 and 5 can cause the simultaneous outage of power and heat capacities. Hence, they correspond to the same capacity outage states, i.e., CS4 in Fig. 3. For readability, the capacity state on outage is written as capacity state for short, and the probability of capacity state on outage is written as outage probability for short.

$$\begin{cases}
\mathbf{P}_{chp} = \begin{bmatrix} P_{chp_0} & P_{chp_h} \\ P_{chp_e} & P_{chp_e\&h} \end{bmatrix} \\
\mathbf{P}_{chp}^* = \begin{bmatrix} 1 & P_{chp_h} + P_{chp_e\&h} \\ P_{chp_e\&h} + P_{chp_e} & P_{chp_e\&h} \end{bmatrix}
\end{cases} (1)$$

Equation (1) represents the outage probability matrix P_{chp} and cumulative outage probability matrix P_{chp}^* of a CHP, corresponding to the capacity outage states in Fig. 3. The capacity state CS1 (0, 0) means all power and heat capacities are available, and its probability is P_{chp} of CS2 (0, H_{chp}) means

the heat capacity is in outage and the power capacity is available, and its probability is P_{chp} ; CS3 (C_{chp} , 0) means the power capacity is in outage and the heat capacity is available, and its probability is P_{chp_e} ; and CS4 (C_{chp} , H_{chp}) means all power and heat capacities are not available, and its probability is $P_{chp \ edh}$, which is the common-cause forced outage rate of CHP. Each element of the 2-D matrix \boldsymbol{O}_{chp} in Fig. 3 is a binary array representing the corresponding power and heat capacity outage states, where C_{chp} is the power supplying capacity of a CHP; and H_{chp} is the heat supplying capacity of a CHP. $\lambda_1^* - \lambda_5^*$ and $\mu_1^* - \mu_5^*$ are the transition rates between different capacity outage states. These outage probabilities can be calculated by the stationary residing probability P_i as shown in (2). As CS4 includes States 4 and 5, $P_{chp_e\&h}$ is calculated by the sum of P_4 and P_5 . It is easy to find that $P_{chp_e\&h}$ is not equal to $P_{chp_e}P_{chp_h}$ in (1). It means the outages of power and heat capacities are not independent dent. Instead, they are dependent due to the existence of the common-cause outage of power and heat capacities in the CHP. Therefore, if the power and heat capacities are modeled separately in a vector, the probability of the simultaneous outage of multiple energy forms would not be expressed. Finally, a multi-dimensional-matrix-based modeling method is proposed to describe the dependent capacity states and the corresponding probability distribution.

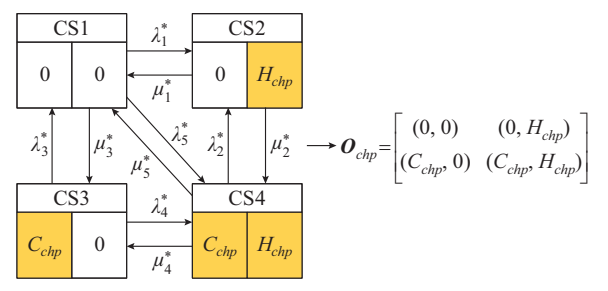


Fig. 3. Diagram of CHP capacity outage state space.

$$\begin{cases} P_{0} = P_{1} \\ P_{chp_e} = P_{3} \\ P_{chp_h} = P_{2} \\ P_{chp_e\&h} = P_{4} + P_{5} \end{cases}$$
(2)

The cumulative probability matrix P_{chp}^* means the probability that one capacity state is above the current state. The cumulative probability of the capacity state (0, 0) is 1, because all other capacity states are all above (0, 0). The sum of the probabilities of all capacity states is always 1.

2) COPT Model of P2H

The P2H is a typical MEC facility which transforms electricity into heat. Electric boilers (EBs) and electric heat pumps (EHPs) are potential to be deployed in northern China to solve the clean heating problem [1], [33]. Therefore, the adequacy study of MEC in the IES is urgently required. Usually, P2H has just two states: normal or failed. But in the normal state, P2H consumes electricity to produce heat, which leads to a dependency between electricity and heat energy systems. The shortage of electricity will cause the outage of its heat capacity, i.e., the energy-shortage-related out-

age of capacity. Therefore, it cannot be modeled individually as a heat capacity or electricity load in the IES capacity model. The 2-D matrix is used to model the dependency inside the MEC by considering the electricity consumption as a dummy capacity.

Specifically, when P2H works normally, it provides an available heat capacity equivalent to a negative heat capacity state. Meanwhile, it consumes power capacity equivalent to a positive power capacity state in the IES. The state is shown in the lower-left corner of O_{P2H} , i. e., $(C_{P2H}, -H_{P2H})$, where O_{P2H} is the matrix representing the outage capacity states of P2H; and C_{P2H} and H_{P2H} are the power and heat outage capacities of P2H, respectively. When P2H is failed, it equals to the zero capacity state in the upper-right corner of O_{P2H} . The corresponding outage probability matrices are represented by O_{P2H} and O_{P2H} are the working and failed probabilities, respectively. The sum of them is 1.

$$\begin{cases}
\mathbf{O}_{P2H} = \begin{bmatrix} (0,0) & (0,0) \\ (C_{P2H}, -H_{P2H}) & (0,0) \end{bmatrix} \\
\mathbf{P}_{P2H} = \begin{bmatrix} 0 & P_{P2H} \\ P_{0_P2H} & 0 \end{bmatrix} \\
\mathbf{P}_{P2H}^* = \begin{bmatrix} 1 & P_{P2H} \\ 1 - P_{P2H} & 0 \end{bmatrix}
\end{cases}$$
(3)

3) COPT Models of Generation and Furnace

A furnace generates heat from natural gas, which is a single-energy generator. Hence, both of them can be modeled by the COPT model of the generation system.

4) COPT Model of Multi-energy Loads

There also exists a correlation among different energy loads [14]. We can use the 2-D matrix to model the multi-energy loads as positive capacity outage states. For example, Fig. 4 shows a six-segment power and heat load curve.

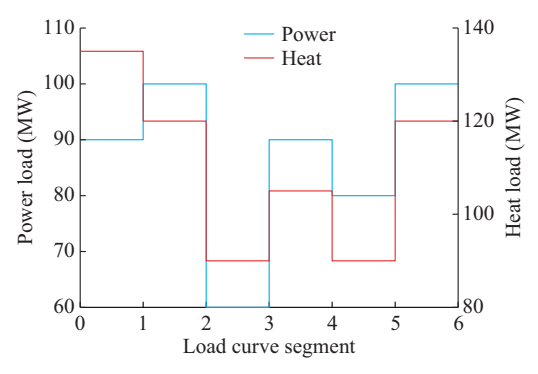


Fig. 4. Six-segment power and heat load curve.

The 2-D matrix size parameter $(N_{L_e}+1)\times(N_{L_h}+1)$ can be determined by (4) based on the maximum power and heat loads $L_{e,\max}$ and $L_{h,\max}$, and capacity increments CI_e and CI_h .

$$\begin{cases} N_{L_e} = \frac{L_{e, \text{max}}}{CI_e} \\ N_{L_h} = \frac{L_{h, \text{max}}}{CI_h} \end{cases}$$
(4)

To calculate the probability matrix P_{l} , we count all these multi-energy load states one by one as illustrated in [24]. The probability of the first load state (90 MW, 135 MW) in Fig. 4 is 1/6. As for P_{I}^{*} , it can be obtained by the Proposition 1 in Section III-A.

B. COPT Model of IES

The COPT model of an IES consists of three 2-D matrices, i.e., $COPT = [O, P, P^*]$, where O is the capacity outage state matrix (COSM) of the IES; P is the capacity outage probability matrix (COPM); and P^* is the cumulative capacity outage probability matrix (CCPM). Their internal structures are shown in Figs. 5-7.

!	0	1	 N
0	(0, 0)	$(0, CI_h)$	 $(0, N \cdot CI_h)$
1	$(CI_e, 0)$	(CI_e, CI_h)	 $(CI_e, N \cdot CI_h)$
:	:	:	:
M	$(M \cdot CI_e, 0)$	$(M \cdot CI_e, CI_h)$	 $(M \cdot CI_e, N \cdot CI_h)$

Fig. 5 Internal structure of COSM.

Fig. 6 Internal structure of COPM.

Fig. 7 Internal structure of CCPM.

All coordinates start from zero, the row coordinates relate to power capacity outage states, and the column coordinates relate to heat capacity outage states. M+1 is the number of all the power capacity outage states; and N+1 is the number of all the heat capacity outage states. In the COSM, CI, and CI_h are the power and heat outage capacity increments, respectively, which make the discrete convolution algorithm practical to the large-scale energy system with facilities of different capacity sizes by discretizing the capacity states; the total heat capacity of the IES is $N \cdot CI_h$; and the total power capacity is $M \cdot CI_e$. Each element of COSM represents one dependent capacity state of an IES, which can be easily calculated by $(i \cdot CI_e, j \cdot CI_h)$, marked as (i, j) for short. P(i,j) in COPM represents the joint probability of the corresponding dependent capacity outage states in an IES. $P^*(i,j)$ in cumulative capacity outage probability matrix (CCPM) is defined as:

$$P^{*}(i,j) = \sum_{m=i}^{M} \sum_{n=j}^{N} P(m,n)$$
 (5)

Note that if the multi-energy loads or P2H are convolved, the capacity outage states can be computed by a conversion of their coordinates.

III. 2-D DISCRETE CONVOLUTION ALGORITHM

Traditional generation system adequacy assessment uses the discrete convolution algorithm to compute its COPT model. Then, the adequacy indices can be obtained after the generation reserve model is computed by convolving the generation model with the load model [24], [25]. However, the traditional method is based on a one-dimensional discrete convolution. To compute the above joint probability distribution, a 2-D discrete convolution algorithm is proposed.

Definition 1 (2-D discrete convolution) [30]: for two 2-D matrices $A_{(M_a+1)\times(N_a+1)}$ and $B_{(M_b+1)\times(N_b+1)}$, their discrete convolution result is denoted by the matrix C, and the computation process can be represented by $C = A \otimes B$.

$$C(i,j) = \sum_{m=0}^{i} \sum_{n=0}^{j} A(m,n)B(i-m,j-n)$$

$$0 \le i \le M_a + M_b, \ 0 \le j \le N_a + N_b$$
(6)

Definition 1 defines the 2-D discrete convolution process. There have been several efficient methods for solving the 2-D discrete convolution problem, which is out of the scope of this paper. This paper focuses on how to apply the 2-D discrete convolution algorithm correctly to compute the COPT of IES and the corresponding adequacy indices.

A. Customized 2-D Discrete Convolution Algorithm

As we usually perform the 2-D discrete convolution algorithm recursively to obtain the final COPT model of an IES, which will be presented in the following computation procedure part, we only need to illustrate how to perform this algorithm on two known COPT models to obtain the new model. Note that we have two known IESs $A_{(M_a+1)\times(N_a+1)}$ and

When integrating B into A, we obtain the new combined system C and its COPT $[O_C, P_C, P_C^*]$.

1) COPM

The element of P_C can be calculated by (7), which is represented compactly by $P_C = P_A \otimes P_B$.

$$P_{C}(i,j) = \sum_{m_{1}+m_{2}=i} \sum_{n_{1}+n_{2}=j} P_{A}(m_{1},n_{1}) P_{B}(m_{2},n_{2}) = \sum_{m=0}^{M_{a}} \sum_{n=0}^{N_{a}} P_{A}(m,n) P_{B}(i-m,j-n)$$

$$0 \le i \le M_{a} + M_{b}, \ 0 \le j \le N_{a} + N_{b}$$

$$(7)$$

There will be some elements with negative coordinates in P_B . Their values are set to be zero, because all coordinates start from zero, which do not exist in the original P_{R} .

CCPM

According to the definition of P^* in (5), we substitute (7) into (5) to obtain (8).

$$P_{C}^{*}(i,j) = \sum_{m=i}^{M_{a}+M_{b}} \sum_{n=j}^{N_{a}} \sum_{p=0}^{N_{a}} \sum_{q=0}^{N_{a}} P_{A}(p,q) P_{B}(m-p,n-q) =$$

$$\sum_{p=0}^{M_{a}} \sum_{q=0}^{N_{a}} \sum_{m=i}^{N_{a}} \sum_{n=j}^{M_{a}+M_{b}} P_{A}(p,q) P_{B}(m-p,n-q) =$$

$$\sum_{n=0}^{M_{a}} \sum_{a=0}^{N_{a}} P_{A}(p,q) P_{B}^{*}(i-p,j-q)$$

$$(8)$$

It can be easily observed that there are several elements whose positive coordinates above the original range of coordinates in P_B^* . Their values are set to be zero. But for those elements with negative coordinates in P_B^* , their values cannot be simply set to be 1 just as the discrete computation for the traditional generation system. Therefore, the key of the computation is to determine the value of $P_B^*(i,y)$ and $P_B^*(y,j)$, where y is a negative integer, $0 \le i \le M_b$, and $0 \le j \le N_b$.

To compute the CCPM P_C^* correctly through the 2-D convolution, the following extension rule for P_B^* is proposed to calculate the correct values for $P_B^*(i,y)$ and $P_B^*(y,j)$, y < 0.

Extension rule: to clarify the new extended matrix, it is renamed as P_B^{**} , then it can be obtained based on the original P_B^* as (9). Figure 8 shows the numerical structure of P_B^{**} .

$$\begin{cases} P_{B}^{**}(i,j) = 1 & 0 \le i < M_{a}, 0 \le j < N_{a} \\ P_{B}^{**}(i,j) = P_{B}^{*}(i-M_{a}, 0) \\ M_{a} \le i \le M_{a} + M_{b} + 1, 0 \le j < N_{a} \\ P_{B}^{**}(i,j) = P_{B}^{*}(0,j-N_{a}) \\ 0 \le i < M_{a}, N_{a} \le j \le N_{a} + N_{b} + 1 \\ P_{B}^{**}(i,j) = P_{B}^{*}(i-M_{a},j-N_{a}) \\ M_{a} \le i \le M_{a} + M_{b} + 1, N_{a} \le j \le N_{a} + N_{b} + 1 \end{cases}$$

$$(9)$$

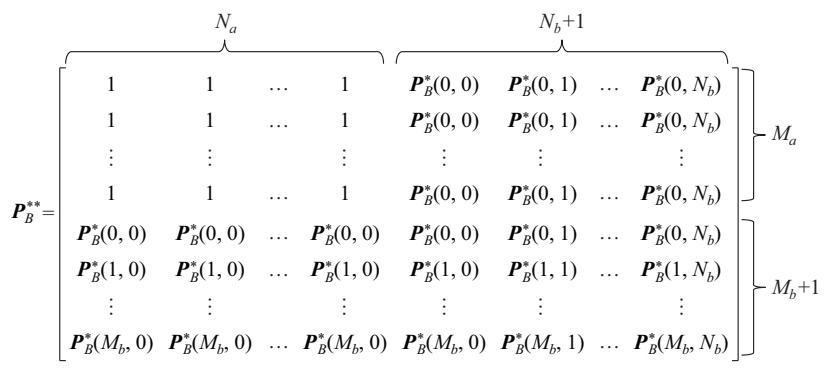


Fig. 8. Numerical structure of P_n^{**}

The computation procedures of CCPM P_C^* are described as follows

- 1) Extend P_B^* to P_B^{**} according to the extension rule.
- 2) Compute $P_A \otimes P_B^{**}$, then select the matrix with the size $(M_a + M_b + 1, N_a + N_b + 1)$ in the lower right of $P_A \otimes P_B^{**}$ as the final P_C^* .

Figure 9 shows the internal structure of $P_A \otimes P_b^{**}$, where $M_b \times N_b$, $M_b \times (N_a + N_b + 1)$, $(M_a + M_b + 1) \times N_b$, and $(M_a + M_b + 1) \times (N_a + N_b + 1)$ are the dimensions of P_0 , P_1 , P_2 , and P_C^* , respectively.

$$\begin{aligned} \boldsymbol{M_b} \times \boldsymbol{N_b} & \boldsymbol{M_b} \times (\boldsymbol{N_a} + \boldsymbol{N_b} + 1) \\ \boldsymbol{P_A} \otimes \boldsymbol{P_B^{**}} = \begin{bmatrix} \boldsymbol{P_0} & \boldsymbol{P_1} \\ \boldsymbol{P_2} & \boldsymbol{P_C^*} \end{bmatrix} \\ \boldsymbol{(M_a + M_b + 1)} \times \boldsymbol{N_b} & \boldsymbol{(M_a + M_b + 1)} \times (\boldsymbol{N_a} + \boldsymbol{N_b} + 1) \end{aligned}$$

Fig. 9. Internal structure of $P_A \otimes P_B^{**}$.

These computation procedures are represented as $\hat{\otimes}$:

$$\boldsymbol{P}_{C}^{*} = \boldsymbol{P}_{A} \, \hat{\otimes} \, \boldsymbol{P}_{B}^{*} \tag{10}$$

Proposition 1: if a 2-D COPM P is known, the corresponding CCPM P^* can be computed as:

$$\boldsymbol{P}^* = \boldsymbol{P} \, \hat{\otimes} \, \boldsymbol{1} \tag{11}$$

This proposition is very useful to calculate P_C^* especially when P_B^* is difficult to obtain. We can first calculate P_C , then

calculate P_c^* by the proposition. Note that the latter method requires more memory space than (10), while its multiplication operations are easier. This property is a very important finding in this paper.

Proof: considering that P_A and P_B^* are known, we want to calculate P_C^* in (10). According to the above definition of $P_A \otimes P_B^*$ and (8), any element of the final computation result of $P_A \otimes P_B^*$ can be written as:

$$P_{C}^{*}(i,j) = \left(P_{A} \hat{\otimes} P_{B}^{*}\right)(i,j) = \sum_{p=0}^{M} \sum_{q=0}^{N} P_{A}(p,q) P_{B}^{*}(i-p,j-q)$$
(12)

Assume the original $P_B^* = 1$, i.e., $P_B^*(0,0) = 1$. According to the definition of P_B^{**} in the above extension rule, if $p \ge i$ and $q \ge j$, $P_B^*(i-p,j-q) = 1$; otherwise, its value is 0. Therefore, (12) can be further replaced by:

$$P_{C}^{*}(i,j) = \left(P_{A} \, \hat{\otimes} \, P_{B}^{*}\right)(i,j) = \sum_{p \ge i}^{M} \sum_{q \ge j}^{N} P_{A}(p,q) \tag{13}$$

According to the definition of P^* in (5), it is clear that $\left(P_A \, \hat{\otimes} \, P_B^*\right)(i,j)$ is exactly $P_A^*(i,j)$. Therefore, $P_C^* = P_A^* = P_A \, \hat{\otimes} \, 1$. So far, the proposition is established.

B. Computation Procedure of COPT of IES for Adequacy Assessment

This subsection describes the procedures to generate the COPT of an IES and compute its adequacy indices. A numerical example is given in Appendix A.

1) Formulation of COPT of Combined Generation and Furnace Systems

Assume that an IES has N_g generators and N_f furnaces. The COPT of the generation system $[\boldsymbol{O}_g, \boldsymbol{P}_g, \boldsymbol{P}_g^*]$ and furnace system $[\boldsymbol{O}_f, \boldsymbol{P}_f, \boldsymbol{P}_f^*]$ can be formulated as the COPT of traditional generation system. The numbers of capacity outage states of COPTs of generation and furnace systems are N_g+1 and N_f+1 , respectively. Note that \boldsymbol{O}_g , \boldsymbol{P}_g , \boldsymbol{P}_g^* are all one-dimensional vectors.

The 2-D COPT of the combined generation and furnace system $[\mathbf{O}_{GF}, \mathbf{P}_{GF}, \mathbf{P}_{GF}^*]$ is as follows:

$$\boldsymbol{P}_{GF} = \boldsymbol{P}_{g}^{\mathrm{T}} \boldsymbol{P}_{f} \tag{14}$$

$$\boldsymbol{P}_{GF}^* = \left(\boldsymbol{P}_g^*\right)^{\mathrm{T}} \boldsymbol{P}_f^* \tag{15}$$

where the subscript GF represents the combined generation and furnace system.

2) Formulation of COPT of CHP System

Assume that the IES has N_{chp} CHPs, and the COPT of the i^{th} CHP is $[\boldsymbol{O}_{chp,i}, \boldsymbol{P}_{chp,i}, \boldsymbol{P}_{chp,i}^*]$ $(i=1,2,...,N_{chp})$. The COPT of each single CHP can be formed as illustrated in Section II-A. Its power and heat capacity increment must be consistent with CI_e and CI_h . The COPT of the whole CHP system $[\boldsymbol{O}_{CHP}, \boldsymbol{P}_{CHP}, \boldsymbol{P}_{CHP}^*]$ can be obtained recursively.

$$\boldsymbol{P}_{CHP,n} = \boldsymbol{P}_{CHP,n} \otimes \boldsymbol{P}_{CHP,n-1} \quad n = 2, 3, ..., N_{CHP}$$
 (16)

$$\mathbf{P}_{CHP,n}^* = \mathbf{P}_{CHP,n-1} \hat{\otimes} \mathbf{P}_{CHP,n}^* \quad n = 2, 3, ..., N_{CHP}$$
 (17)

3) Formulation of COPT of an IES

The COPT of an IES $[\boldsymbol{O}_{IES}, \boldsymbol{P}_{IES}, \boldsymbol{P}_{IES}^*]$ can be formulated as (18) and (19). The dimensions of $\boldsymbol{O}_{IES}, \boldsymbol{P}_{IES}$, and \boldsymbol{P}_{IES}^* are all $(N_{IES_a}+1)\times(N_{IES_b}+1)$.

$$\boldsymbol{P}_{IES} = \boldsymbol{P}_{GF} \otimes \boldsymbol{P}_{CHP} \tag{18}$$

$$\boldsymbol{P}_{IES}^* = \boldsymbol{P}_{GF} \, \hat{\otimes} \, \boldsymbol{P}_{CHP}^* \tag{19}$$

4) Convolution of IES with Multi-energy Loads

$$\boldsymbol{P}_{L}^{*} = \boldsymbol{P}_{L} \hat{\otimes} \mathbf{1} \tag{20}$$

$$\boldsymbol{P}_{IESL} = \boldsymbol{P}_{IES} \otimes \boldsymbol{P}_{L} \tag{21}$$

$$\boldsymbol{P}_{IESL}^* = \boldsymbol{P}_{IES} \, \hat{\otimes} \, \boldsymbol{P}_L^* = \boldsymbol{P}_L \, \hat{\otimes} \, \boldsymbol{P}_{IES}^*$$
 (22)

where the subscript *IES* is the model that only includes generations; and the subscript *IESL* is the model that includes generations and loads in the IES, which can be called IES reserve model.

The COPM of multiple-loads P_L can be formed according to the multi-load model in Section II-A, then CCPM P_L^* can be obtained in (20) by applying Proposition 1. We use (21) and (22) to convolve the IES with the multi-energy loads. The internal structure of the CCPM of integrated energy system with load (IESL) is given in Fig. 10, whose size is $(N_{IES_L} + N_{L_1} + 1) \times (N_{IES_L} + N_{L_1} + 1)$.

To calculate the capacity outage states in the IES reserve model, a coordinate conversion is defined as:

$$O_{IESL}(i,j) = \left((i - N_{IES_e}) \cdot CI_e, (j - N_{IES_h}) \cdot CI_h \right)$$

$$0 \le i \le N_{IES_e} + N_{L_e}, 0 \le j \le N_{IES_h} + N_{L_h}$$
(23)

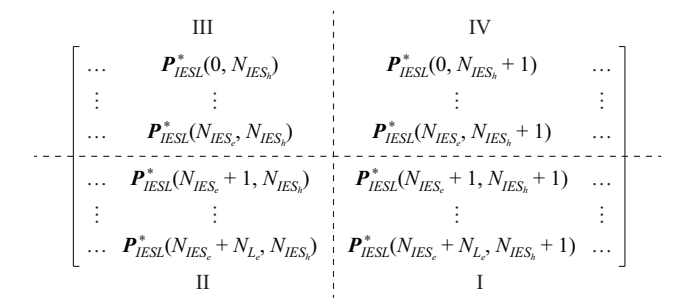


Fig. 10. Internal structure of CCPM of IESL.

5) Calculation of Adequacy Indices of an IES

The proposed adequacy indices of an IES and their computation methods are shown in Table I. $LOLP_{e||h}$ is a whole adequacy index for an IES indicated by parts I, II, and IV in Fig. 10. Part I represents the united loss of power and heat load $LOLP_{e\&h}$. Part II states that there is only power loss $LOLP_{e}$. Part IV states that there is only heat loss $LOLP_{h}$. Part III means that there is no heat or power loss. The whole index is not the direct sum of adequacy indices of different energy systems, which is calculated as $LOLP_{e||h} = LOLP_{e} + LOLP_{h} + LOLP_{e\&h}$ instead. For example, if an IES sheds power and heat loads during 1 hour at the same time, the duration of load shedding for the whole system is not 2 hours but 1 hour. The related probability adequacy index LOLE, i.e., the loss of load expectation, can be calculated by $LOLE = LOLP \times 8760$.

TABLE I ADEQUACY INDICES FOR AN IES

Index	Interpretation	Computation
$LOLP_{e\&h}$	Probability of power and heat load losses	$LOLP_{e\&h} = P_{IESL}^* \left(N_{IES_e} + 1, N_{IES_h} + 1 \right)$
$LOLP_e$	Probability of only power load loss	$LOLP_e = P_{IESL}^*(N_{IES_e} + 1,0) - LOLP_{e\&h}$
$LOLP_h$	Probability of only heat load loss	$LOLP_h = P_{IESL}^*(0, N_{IES_h} + 1) - LOLP_{e\&h}$
$\mathit{LOLP}_{e h}$	Probability of power or heat load loss	$LOLP_{e h} = LOLP_h + LOLP_e + LOLP_{e\&h}$
EENS (MWh/year)	Expected electricity not served	
EHNS (MWh/year)	Expected heat not served	

C. 2-D Discrete Convolution Algorithm with Integration of P2H

P2H facility can work when there is adequate power. In the above adequacy study, after the IES model is convolved with the load model, there will be some capacity outage states of $C_e < 0$ and $C_h > 0$ in the generated IES reserve model O_{IESL} . These states mean that there is excessive power supply but the heat load is not served, and all of these states are stated as EOHL. The COSM of these states is represented by O_{EOHL} , and their COPM is represented by P_{EOHL} , which means the outage probability matrix of all capacity states on electricity excessive and heat loss. We can extract the P_{EOHL} corresponding to EOHL from the original P_{IESL} , which has

been obtained above.

To facilitate the computation, we divide all P2H facilities into $N_{\rm COP}$ groups according to the coefficient of performance (COP).

Definition 2 (COP): COP is the ratio of work or useful output to the amount of work or energy input, generally used as a measure of the energy efficiency of air conditioners, space heaters and other cooling and heating devices.

The COP in Definition 2 is the ratio of heat energy output to electricity energy input. The COP of the EB is very close to 1, which means that it nearly converts all the power into heat energy and the COP of the electric heat pump (EHP) is above 1. They are usually assumed to be constants in the research field. Specifically, the P2H facilities with similar COPs are put in the same group. The COPM of P2H in the i^{th} group is denoted by $P_{P2H(i)}$. For example, there are two EHPs with the power input capacity of 10 MW, the heat output capacity of 15 MW, the same COP of 1.5, and the outage probability of 0.05. They are put together into the first group, and their COPM $P_{P2H(1)}$ is formulated together by 2-D convolution, as presented in Appendix A Table A-X. If the IES has one additional EHP with power input capacity of 10 MW, heat output capacity of 30 MW, and COP of 3, and the outage probability of 0.05, it is separately as the second group of P2Hs, whose COPM $P_{P2H(2)}$ is in Appendix A Table A-X.

Then, P2H can be committed in EOHL to reduce the heat loss in EOHL. EOHL can be regarded as a condition of using P2H in adequacy assessment. Here, it is considered as an event represented by E_{EOHL} . Further, the impact of P2H on the adequacy of IES can be computed in a conditional probability approach. Specifically, the employment of P2H reduces heat loss in EOHL, which is regarded as the event E_{P2H} . When P2H is considered, the COPM of EOHL will also be changed. We regard the new COPM of EOHL after the employment of P2H as $P_{EOHL&P2H}$. However, P2H is only employed when the event E_{EOHL} occurs. The conditional employment of P2H can be regarded as a conditional event $(E_{P2H}|E_{EOHL})$. Following the logistic of the conditional probability, $P_{EOHL&P2H}$ could be calculated by (24).

$$P(E_{P2H}) = P(E_{P2H}|E_{EOHL}) \otimes P(E_{EOHL}) = P_{P2H} \otimes P_{EOHL}$$
 (24)

However, the P2H is assumed to operate at full capacity in (24). In reality, as the operation of P2H depends on the power supply, if there is not enough power supply, P2H might operate at its full capacity or partial capacity. The consequence is that (24) will generate some capacity states with positive power capacity outage O_e , i. e., $O_e > 0$. However, these states do not actually exist, because P2H would not be employed when there is a shortage of electricity in the IES. For a numerical example, Appendix A Table A-IX has P_{FOHL} of EOHL, which is extracted from Table A-VI. Then, the above first group of P2Hs is employed to improve the heat loss in EOHL. When convolving the last row of P_{EOHL} in Table A-IX that corresponds to the power capacity outage of -10 MW with the last row of $P_{P2H(1)}$ in Table A-X that corresponds to the heat capacity outage of 20 MW, a new power capacity outage of 10 MW will be generated. It means that the system just has an extra 10 MW power capacity, but it is employed to drive the first group of EHPs at the full capacity of 20 MW. Finally, a non-existent -10 MW capacity state is created. The reality is that the extra 10 MW can drive the P2H of 10 MW to work. Hence, $P_{EOHL\&P2H} \neq P(E_{P2H})$. A numerical example of $P(E_{P2H})$ is given in Appendix A Table A-XI.

To cope with the problem, a row-by-row convolution algorithm (MEC convolution algorithm) is proposed. The idea behind the algorithm is that when encountering a row which generates the non-existent capacity states, the probabilities of the corresponding capacity states of P2H are merged into the nearest existing capacity states. For example, when the last row of P_{EOHL} is convolved with $P_{P2H(1)}$, the probability of (20 MW, 30 MW) is integrated into (10 MW, 15 MW) in $P_{P2H(1)}$. Meanwhile, the row with power capacity outage of 20 MW in $P_{P2H(1)}$ is neglected. Finally, the correct $P_{EOHL\&P2H}$ can be calculated by the algorithm and shown in Appendix A Table A-XII.

The proposed MEC convolution algorithm consists of three subparts. The first subpart initializes all parameters. There are N_{COP} groups of P2H facilities in total. The maximum power and heat capacities of the ith group of P2H (P2H(i)) are $N_{P2He(i)} \cdot CI_e$ and $N_{P2Hh(i)} \cdot CI_h$, respectively. The COPM of the i^{th} group of P2H is $P_{P2H(i)}$. Considering the zero capacity outage states, the size of $P_{P2H(i)}$ should be $(N_{P2He(i)} + 1) \times (N_{P2Hh(i)} + 1)$. Considering the coordinates of the matrix starting from 0, its coordinates should start from (0,0) to $(N_{P2He(i)}, N_{P2Hh(i)})$. We initialize $P_{IESL\&P2H}$ to be P_{IESL} . Then P_{EOHL} is extracted from $P_{IESL\&P2H}$ whose size is $(N_{IESe} + N_{Le} +$ 1)× $(N_{IESh} + N_{Lh} + 1)$ given in Section III. The maximum power and heat capacities of the EOHL are $N_{EOHLe} \cdot CI_e$ and $N_{EOHLh} \cdot$ CI_h , respectively. The COPM of EOHL is P_{EOHL} with its size of $N_{EOHLe} \times N_{EOHLh}$. Its coordinates start from (0,0) to $(N_{EOHLe} 1, N_{EOHLh} - 1$). Note that there are no zero capacity outage states in P_{EOHL} .

In the second subpart, the row-by-row convolution is computed. Considering the employment of the ith group of P2H facilities, the COPM of P_{EOHL} is updated to $P_{EOHL\&P2H(i)}$. As $P_{EOHL\&P2H(i)}$ will include an additional zero power outage capacity, its size on power capacity outage should be $N_{EOHLe} + 1$, and the size on heat capacity $N_{EOHLh} + N_{P2Hh(i)} + 1$. Therefore, its coordinates start from (0,0)to $(N_{EOHLe}, N_{EOHLh} + N_{P2Hh(i)})$. Specifically, we first find the part of P_{EOHL} , which can be convolved with $P_{P2H(i)}$ but does not generate the non-existent power capacity outage states. The corresponding row coordinate l_0 can be calculated by l_0 = $N_{EOHLe} - N_{P2He(i)}$. After that, for the remaining rows with the coordinates larger than l_0 , they are convolved with $P_{P2H(i)}$ one by one. The coordinate that is currently convolved is l_{EOHL} . When convolving the row with $P_{P2H(i)}$, we consider the P2H operating at partial capacity by merging the probability of those impossible capacity states of P2H into the nearest feasible capacity states in $P_{P2H(i)}$. The process is achieved by a very skillful recursive equation, which will be presented in (28). The equation copes with the situation where P2H might operate at partial capacity when the electricity is inadequate, which is thus the core of the algorithm. In (28), $(x-1,y+CI_e\cdot COP_i/CI_h)$ is the coordinate of the nearest feasible capacity states in $P_{P2H(i)}$ for the currently convolved row l_{EOHL} . It must be stressed that we need elaborately choose the values of CI_e and CI_h to guarantee $CI_e\cdot COP_i/CI_h$ as an integer for each COP_i . For example, $COP_1=1$, $COP_2=1.5$, and $COP_3=3$. We can set $CI_e=1$ MW and $CI_h=0.5$ MW to satisfy the requirement. Finally, we need to integrate the convolution result of the row into $P_{EOHL\&P2H(i)}$.

In the third part, we will modify the original P_{IESL} to $P_{IESL\&P2H}$ according to $P_{EOHL\&P2H(i)}$ considering the impact of P2H(i). Specifically, the employment of P2H(i) changes the original outage probability distribution. We find the corresponding coordinates and adjust the corresponding probabilities.

After repeating the above procedures for all P2H groups, the final COPM $P_{IESL\&P2H}$ considers the impact of all P2H groups on the IES adequacy.

The MEC convolution algorithm is described as follows.

1) Initial Computation (First Subpart)

Step 1: formulate N_{COP} groups of P2H with similar COPs, and calculate the COPM $P_{P2H(i)}$ $(i=1,2,...,N_{COP})$ of each group by 2-D discrete convolution algorithm. Set $P_{IESL\&P2H} = P_{IESL}$. The information of P_{IESL} can be found in Section III. Reset i=0

Step 2: extract P_{EOHL} from $P_{IESL\&P2H}$ by (25). Meanwhile, clear the corresponding probabilities in $P_{IESL\&P2H}$ by (26). Update i = i + 1

$$P_{EOHL}(0:N_{EOHLe} - 1, 0:N_{EOHLh} - 1) = P_{IESL\&P2H}(0:N_{IESe} - 1, N_{IESh} + 1:N_{IESe} + N_{IESh})$$
(25)

$$P_{IESL\&P2H}(0:N_{IESe}-1,N_{IESh}+1:N_{IESe}+N_{IESh})=\mathbf{0}$$
 (26)

2) Convolution Computation (Second Subpart)

Step 3: set $l_0 = N_{EOHLe} - N_{P2He(i)}$, and calculate $P_{EOHL\&P2H}$ without generating the non-existent capacity states by (27). Note that the coordinates of matrix start from 0.

$$\boldsymbol{P}_{EOHL\&P2H} = \boldsymbol{P}_{P2H}(i) \bigotimes \boldsymbol{P}_{EOHL}(0:l_0,0:N_{EOHLh}-1)$$
 (27)

Step 4: record the coordinate of the lower left corner of $P_{P2H(i)}$, $x=N_{P2He(i)}-1$, y=0; for the remaining part of P_{EOHL} , convolve them with $P_{P2H(i)}$ in the row order.

Step 5: set the coordinate of the current row convolved in P_{EOHL} , i.e., $l_{EOHL} = N_{EOHLe} + 1 - x$; $l_{P2H} = x - 1$ is the row coordinate of the corresponding row in $P_{P2H(i)}$ to guarantee that there are not positive power capacity outage states generated.

Step 6: for those rows with the coordinates larger than l_{P2H} in $P_{P2H(i)}$, merge their probabilities into the nearest feasible capacity states in the row l_{P2H} by (28). It is a recursive operation considering all non-existent capacity states and copes with the operation of P2H with partial capacity.

$$P_{P2H(i)}(x-1,y+CI_{e}\cdot COP_{i}/CI_{h}) = P_{P2H(i)}(x,y) + P_{P2H(i)}(x-1,y+CI_{e}\cdot COP_{i}/CI_{h})$$
 (28)

Step 7: convolve the row l_{EOHL} of P_{EOHL} with the corresponding $P_{P2H}(i)$ by (29).

$$TEMP = P_{EOHL}(l_{EOHL}, 0:N_{EOHLh} - 1) \otimes P_{P2H(i)}(0:l_{P2H}, 0:N_{P2Hh(i)})$$
 (29)

Step 8: integrate **TEMP** into $P_{EOHL\&P2H(i)}$.

$$\mathbf{P}_{EOHL\&P2H(i)}(l_{EOHL}:N_{EOHLe}, 0:N_{EOHLh} + N_{P2Hh(i)}) = \mathbf{TEMP} + \mathbf{P}_{EOHL\&P2H(i)}(l_{EOHL}:N_{EOHLe}, 0:N_{EOHLh} + N_{P2Hh(i)})$$
(30)

Step 9: modify the coordinate (x, y) by:

$$\begin{cases} x = x - 1 \\ y = y + CI_e \cdot COP_i / CI_h \end{cases}$$
 (31)

Step 10: if x = 0, go to Step 11; otherwise, return to Step 5.

3) Modification Computation (Third Subpart)

Step 11: the size of $P_{EOHL\&P2H(i)}$ is $(N_{EOHLe} + 1) \times (N_{EOHLh} + N_{P2Hh}(i) + 1)$. Modify $P_{IESL\&P2H}$ according to (32):

$$\mathbf{P}_{IESL\&P2H(i)}(0:N_{EOHLe}, N_{IESh} + N_{Lh} - N_{EOHLh} - N_{P2Hh(i)}:
N_{IESh} + N_{Lh}) = \mathbf{P}_{EOHL\&P2H(i)} + \mathbf{P}_{IESL\&P2H(i)}(0:N_{EOHLe},
N_{IESh} + N_{Lh} - N_{EOHLh} - N_{P2Hh(i)}:N_{IESh} + N_{Lh})$$
(32)

Step 12: if $i=N_{COP}$, calculate (33); otherwise, go to Step 2.

$$\boldsymbol{P}_{IESI\&P2H}^* = \boldsymbol{P}_{IESI\&P2H} \hat{\otimes} 1 \tag{33}$$

D. Flowchart of Evaluation Procedure of Capacity Adequacy

The overall evaluation procedure of capacity adequacy for the IES is summarized as the flowchart in Fig. 11.

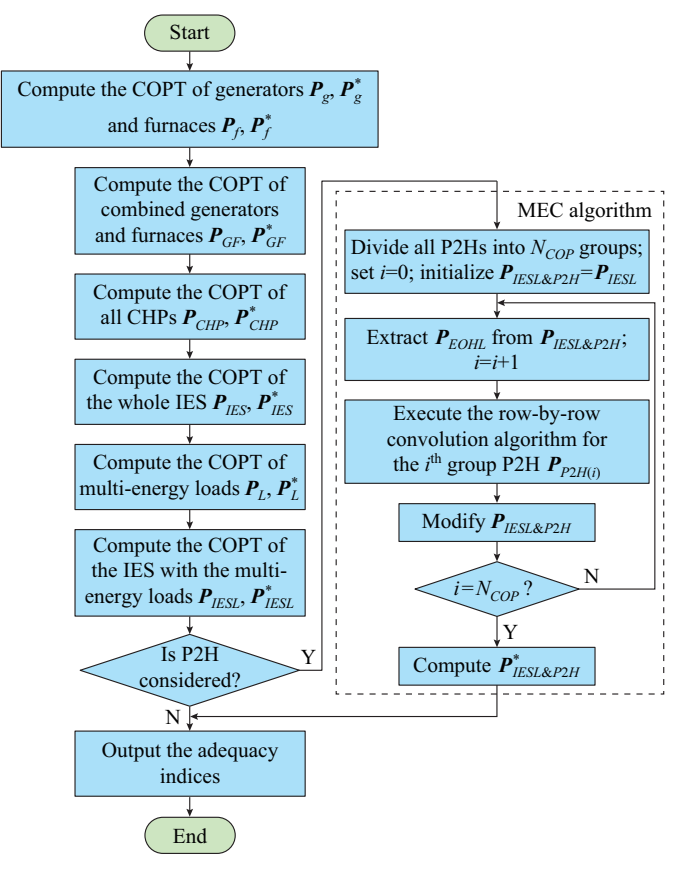


Fig. 11. Overall evaluation procedure of capacity adequacy for IES.

IV. CASE STUDY

In this section, we adopt the SEM, which is a basic analytical method, to validate the correctness of the proposed algorithm. Here, we enumerate all possible states without any truncation of the state space. After illustrating the correctness of the proposed algorithm, we use it to study the capacity of P2H, which could give technical references for the op-

erator or investor on how many P2H facilities can be deployed in a wind-IES in a quantitative way. The discrete-convolution-based COPT method has been successfully applied to the adequacy evaluation of large-scale generation system. A mid-scale IES is used as the case study to prove the correctness of the algorithm.

The basic data of the considered IES are given in Table II. The specific power load data L_e and heat load data L_h are shown in (34), and are also shown in Fig. 4.

TABLE II DATA OF TEST IES

C_g (MW)	P_g	C_{chp} (MW)	H _{chp} (MW)	$P_{chp_e\&h}$	$H_f(MW)$	P_f
10	0.05	10	15	0.05	30	0.05
10	0.05	10	15	0.05	30	0.05
10	0.05	20	30	0.05		
20	0.01	20	30	0.01		

$$\begin{cases}
L_e = (90, 100, 60, 90, 80, 100) \text{MW} \\
L_h = (135, 120, 90, 105, 90, 120) \text{MW}
\end{cases}$$
(34)

A. Adequacy Evaluation of IES

In this case, CI_e and CI_h are both set to be 5 MW. These adequacy indices are shown in Table III. It can be found that there are 23.32 days ($LOLE_{e|h} = 0.0639 \times 365$) in load loss (power or heat load loss) of the regional IES in the whole year. And there are 2.62 days ($LOLE_{e\&h}$) in the power and heat load loss at the same time. There are 10.59 days ($LOLE_e$) with only power load loss instead of heat. There are 10.07 days ($LOLE_h$) with only heat load loss instead of power. The power and heat losses of the IES are 3.85×10^3 MWh and 5.77×10^3 MWh in one year, respectively. In Table III, β is the coefficient of variation (COV) representing the ratio of the standard deviation to the average of one index. $\beta = 1\%$ and $\beta = 5\%$ are chosen as the convergence criteria for the EHNS index in MCS.

TABLE III
ADEQUACY INDICES FOR IES

Method	$LOLP_{e\&h}$	$LOLP_{e h}$	$LOLP_h$	$LOLP_e$	EENS (MWh/ year)	EHNS (MWh/ year)
IES COPT	0.0072	0.0639	0.0276	0.0290	3.85×10^{3}	5.77×10^{3}
SEM	0.0072	0.0639	0.0276	0.0290	$3.85\!\times\!10^3$	5.77×10^3
MCS $(\beta = 5\%)$	0.0067	0.0631	0.0267	0.0295	$3.85\!\times\!10^3$	5.57×10^3
MCS ($\beta = 1\%$)	0.0072	0.0641	0.0277	0.0291	3.86×10^{3}	5.78×10^3

 $LOLP_{e\&h}$ and $LOLP_{e||h}$ are indices considering the correlation of multi-energy system. The adequacy index for a single power system is $(LOLP_e + LOLP_{e\&h})$. The adequacy index for a single heat system is $(LOLP_h + LOLP_{e\&h})$. It can be found that the adequacy index for an IES is not the simple summation of individual power and heat energy systems, i. e., $LOLP_{e||h} \neq (LOLP_h + LOLP_{e\&h}) + (LOLP_e + LOLP_{e\&h})$, due to the existing common-cause outage of the CHP system. Con-

sidering this common-cause outage, the equation $LOLP_{e|h} = LOLP_h + LOLP_e + LOLP_{e\&h}$ will be established, which can be validated by the data in Table III. $LOLP_{e\&h}$ and $LOLP_{e|h}$ reflect the impact of the common-cause outage on adequacy.

To validate the correctness of the proposed COPT model, these indices are also calculated by the SEM. The SEM is the basic analytical method that enumerates and assesses each possible system state, and collects all assessment results to obtain the adequacy indices [34]. By enumerating all possible states without any truncation for the state space, the exact values of adequacy indices of the IES considering the multi-energy correlation can be obtained at the price of a huge computation burden. For example, a system with 15 two-state components has 2¹⁵ possible states. In addition, we also compare these methods with MCS method, which is another popular evaluation method for power system reliability.

The results in the second row in Table III show the exact values of the adequacy indices of the IES from SEM. Compared with the results from the first row, we can find that the IES COPT model can calculate the correct adequacy indices. In other words, the 2-D convolution algorithm can calculate the correct indices as the SEM. The results also show that the smaller β is, the closer the indices of MCS are to the exact values. Also, the IES COPT can present dependent multi-energy capacity outage states and their joint outage probabilities.

Next, the proposed row-by-row energy conversion facility convolution algorithm based on conditional probability is validated by the SEM. We assume that the IES has two additional P2H facilities in Table IV. Here, the SEM can also obtain the exact indices of the IES with the deployment of P2H through a conditional judgment in the enumeration process. Specifically, the SEM method needs to make a judgment on each state whether the P2H is employed. The standard is whether the system state has heat load loss and excessive power capacity. If not, P2H will not be used in the state assessment. We still enumerate all states of the IES with the consideration of the P2H states to get the exact adequacy indices.

TABLE IV
DATA OF TWO P2H FACILITIES

P2H	C_{P2H} (MW)	H_{P2H} (MW)	P_{P2H} (MW)
P2H 1	10	10	0.1
P2H 2	10	10	0.1

Those adequacy indices considering the impact of P2H from the IES COPT, SEM, and MCS methods are listed in Table V. Their indices are just slightly different. This validates the correctness of our proposed algorithm. Comparing the results of Tables III and V, the adequacy indices of the power system remain the same, because the P2H would not have any impact on the power load loss. But the installation of P2H can improve the adequacy of the heat system with the EHNS decreasing to 4.03×10^3 MWh/year. It can be found that the heat energy loss is reduced by about 30%

compared with the case without P2H. The indices of MCS with $\beta = 1\%$ are more accurate, but it needs to sample nearly 5 million samples and spends 322 s to finish the calculation. Further, we will compare the computation performances of these algorithms in Section IV-C.

TABLE V
ADEQUACY INDICES FOR IES CONSIDERING P2H

Method	$LOLP_{e\&h}$	$LOLP_{e h}$	$LOLP_h$	$LOLP_e$	EENS (MWh/ year)	EHNS (MWh/ year)
IES COPT	0.0072	0.0544	0.0180	0.0290	3.85×10^{3}	4.03×10^{3}
SEM	0.0072	0.0543	0.0180	0.0290	$3.85\!\times\!10^3$	$4.02\!\times\!10^3$
MCS $(\beta = 5\%)$	0.0063	0.0547	0.0186	0.0298	3.83×10^3	3.90×10^3
MCS $(\beta = 1\%)$	0.0072	0.0544	0.0181	0.0291	$3.85\!\times\!10^3$	$3.98\!\times\!10^3$

B. Capacity Values of P2H in IES

As the P2H is dependent on the power system, it is difficult to assess how many P2Hs are enough to guarantee the reliability of heat supply. Especially, electric heating is becoming a promising option to integrate wind energy and reduce green-house gas emission [33]. If we use many P2H facilities in some areas with rich wind resources to supply heat, how many P2Hs can be deployed? To answer this problem, the capacity value of P2H is studied as follows.

The capacity value of P2H measures the contribution of P2H to the adequacy of the heating system. In general, equivalent firm capacity (EFC) [35] and effective load carrying capability (ELCC) [36] are the two most common definitions of capacity value in the power system. In principle, these definitions are similar, which both replace the fluctuating wind output with an equivalent firm conventional generation capacity on adequacy.

The capacity value helps in a quantitative manner to know the role which the energy conversion facility is playing on the adequacy of an IES. In this case study, the stochastic output of wind farms is considered. Specifically, the reliability model of wind farms with stochastic output is constructed as a discrete multi-state output model by COPT [26], [27]. The total rated capacity of the wind farm is 30 MW in Table VI. The capacity states in Table VI are not the outputs of the wind farm but the capacity on outage, which can be calculated by the rated capacity of the wind farm less its outputs.

TABLE VI COPT OF WIND FARM

O_{wind} (MW)	P_{wind}	P_{wind}^*
0	0.05	1.00
5	0.10	0.95
10	0.20	0.85
15	0.20	0.65
20	0.15	0.45
25	0.10	0.30
30	0.20	0.20

Figure 11(a) shows the EHNS with the addition of P2Hs,

while Fig. 11(b) shows the change of the EHNS with the addition of the firm furnaces. The capacity values corresponding to different P2Hs can be obtained by comparing the adequacy results in Fig. 11. They are directly shown in Table VII. The capacity values do not present a linearly increasing trend with the addition of P2Hs. Even after the addition of the 4th P2H, the capacity values do not increase. The reason is that the heat supply of P2H is restricted by inadequate power supply.

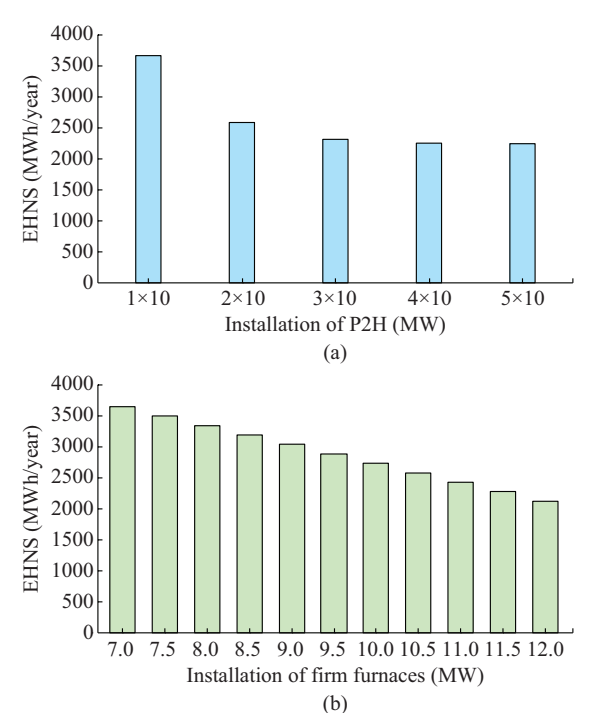


Fig. 11. Adequacy indices of IES with different heating facilities. (a) Adequacy indices with P2H. (b) Adequacy indices with firm furnaces.

TABLE VII CAPACITY VALUES OF P2HS

Installation of P2H (MW)	Capacity value (MW)
1×10	7.0
2×10	10.5
3×10	11.0
4×10	11.5
5×10	11.5

In Fig. 12, the impacts of the power sector on the capacity values of P2H are studied. Specifically, 2×10 MW P2Hs are deployed, but the available generation capacities of the power system are different. It can be found that for the same amount of P2Hs, its capacity value will increase with more power supply. Meanwhile, the EHNS is still decreasing with the increase of power supply. This reflects the impact of the power system on the adequacy of the heating system by the employment of P2H. However, the impact is not linearly dependent on the increase of power supply, which is a system-specific problem. Therefore, a quantitative assessment for the problem is necessary.

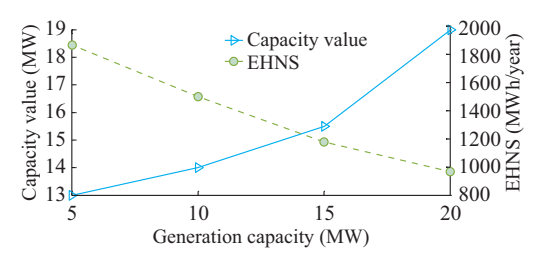


Fig. 12. Adequacy indices of IES with P2Hs and firm furnaces.

C. Computation Performance

The case study verifies the following problem of computation. The SEM and the COPT are both analytical methods to calculate the generation adequacy, but the COPT method has several advantages over the SEM on computation. As it is known, the SEM encounters a very huge computation burden due to the dimension disaster in state space if we enumerate all states in state space. Although the COPT method also enumerates the states in state space, in the recursive convolution process, it can release the computation burden by merging many similar capacity states. Hereby, the wind farm and six 10 MW P2H units are put into the IES system. The capacity increments of CI_e and CI_h for the 2-D convolution method are both 5 MW. The test is performed on a personal computer with Intel core 2.3 GHz and 4 GB memory.

Because of the conditional use of P2H, the total number of the enumerated states cannot be determined before completing the computation. It can be determined numerically after the state enumeration with conditional judgment. For the test system, as shown in Table VIII, the total number of enumerated states is 653772. The final computation time shows that the IES COPT is about 200 times faster than the SEM.

This verifies that the proposed IES COPT algorithm still has the computation advantage over the SEM as the traditional generation system COPT does. Meanwhile, the MCS (β =1%) needs to sample nearly 9 million states and take 555 s to satisfy the convergence requirement. Even though the MCS with β =5% costs a similar time as the SEM, its accuracy of the index is worse. Therefore, in the mid-scale system, the proposed COPT method has an advantage in computation speed and accuracy.

TABLE VIII
COMPUTATION TIME OF SEM AND COPT

Method	Time (s)	Number of states
IES COPT	0.01939	
SEM	5.511	653772
MCS $(\beta = 5\%)$	5.202	365200
MCS $(\beta = 1\%)$	555	8734560

We also apply these methods to a large-scale system including P2H, which has been extended three times in scale to the test system in Section IV-A as well as the load level. The parameters of wind farms in Section IV-B are directly used. The results in Table IX show that the IES COPT method still performs better than other methods. The MCS method samples more states and needs more time to converge than the previous case of mid-scale system. The SEM method cannot get exact indices even after spending 3 hours. Compared with other methods, our proposed method can calculate the exact indices in less than 2 s. Therefore, our method can cope with the large-scale system, but SEM does not work for it.

TABLE IX
COMPUTATION PERFORMANCES OF LARGE-SCALE SYSTEM

Method	$LOLP_{e\&h}$	$LOLP_{e h}$	EENS (MWh/year)	EHNS (MWh/year)	Time (s)	Number of states
IES COPT	4.98×10^{-4}	0.0101	801.0	535.0	1.5	
MCS $(\beta = 5\%)$	4.47×10^{-4}	0.0106	789.3	482.4	90.0	118×10^{4}
MCS $(\beta = 1\%)$	5.02×10^{-4}	0.0102	811.0	530.0	1800.0	270×10 ⁵

As the IES COPT can provide an IES reserve model after the integration of multi-energy loads within short computation time, it can be applied to an on-line decision of reserve capacity or an operation decision.

V. CONCLUSION

This paper presents an analytical method based on COPT to construct the capacity reliability model of an IES for adequacy evaluation. The proposed model considers the impact of multi-energy correlations by multi-dimensional matrices. A customized 2-D discrete convolution algorithm is designed to calculate the IES COPT correctly and fast. Also, the algorithm is improved to consider the impact of P2H by a conditional probability approach. Finally, the methodology can quantify the adequacy of different forms of energy supplies in an IES considering inherent multi-energy correlations, dependent outage, and correlated multi-energy loads. The cor-

rectness of the method is validated by a standard analytical method SEM, which can get the exact adequacy indices. The capacity value of P2H is also studied. The verification of the computation performance shows that the IES COPT maintains the computation advantage over the SEM and MCS as the generation system COPT. Especially, it can calculate the result fast even when the SEM cannot get the result.

The proposed method can be applied to a more complex IES with power, heating, cooling, and gas with consideration of their correlations. This requires multi-dimensional matrix modeling and the corresponding convolution algorithms. For example, the Helix transform [37], which can transform 2-D convolution into 1-D convolution, or other 2-D convolution transformation methods [38], can support the computation of COPTs of the more complex IES systems, e.g., the cooling-heating-power IES or the power-heating-gas IES. Besides, the current study only focuses on the probability indices of an IES ignoring the frequency indices, e.g., loss of load fre-

quency (LOLF). We will develop the proposed method to calculate the frequency indices considering the multi-energy correlations.

APPENDIX A

This is an illustrative numerical example of the procedures for calculating the IES COPT. Specifically, the system is composed of two generators (C_g : 10 MW, P_g : 0.1), one furnace (H_f : 15 MW, P_f : 0.1) and one CHP (C_{chp} : 10 MW, H_{chp} : 15 MW, and $P_{chp_e\&h}$: 0.1). P_{chp_e} and P_{chp_h} are neglected here. The load is a two-segment model with electricity load (10, 20)MW and heat load (15, 15)MW. $CI_e = 10$ MW, $CI_h = 15$ MW. Following the conventions of the above text, the rows of matrix relate to power capacity outage, and the columns of matrix relate to heat capacity outage.

1) Formulation of COPT of Combined Generation and Furnace Systems

TABLE A-I COPT MODEL OF GENERATION AND FURNACE SYSTEMS

O_g (MW)	P_g	P_g^*	O_f (MW)	P_f	P_f^*
0	0.81	1.00	0	0.9	0.9
10	0.18	0.19			
20	0.01	0.10	15	0.1	0.1

TABLE A-II COPT MODEL OF GF SYSTEM

C_{P2H}		P_{GF}	P_{GF}^{*}		
(MW)	$H_{P2H}=0$	$H_{P2H} = 15 \text{ MW}$	$H_{P2H}=0$	$H_{P2H} = 15 \text{ MW}$	
0	0.729	0.081	1.00	0.100	
10	0.162	0.018	0.19	0.019	
20	0.009	0.001	0.01	0.001	

2) Formulation of COPT of CHP System

TABLE A-III COPT MODEL OF CHP SYSTEM

C_{P2H} _		$P_{\it CHP}$	P_{CHP}^*		
(MW)	$H_{P2H}=0$	$H_{P2H} = 15 \text{ MW}$	$H_{P2H}=0$	$H_{P2H} = 15 \text{ MW}$	
0	0.9	0.0	1.0	0.1	
10	0.0	0.1	0.1	0.1	

3) Formulation of COPT of IES

TABLE A-IV COPT MODEL OF IES

		P_{IES}			P_{IES}^*		
C_{P2H} (MW)	$H_{P2H}=0$	$H_{P2H} = 15$ MW	$H_{P2H} = 30$ MW	$H_{P2H}=0$	$H_{P2H} = 15$ MW	$H_{P2H} = 30$ MW	
0	0.6561	0.0729	0.0000	1.000	0.1900	0.0100	
10	0.1458	0.0891	0.0081	0.271	0.1171	0.0100	
20	0.0081	0.0171	0.0018	0.028	0.0199	0.0019	
30	0.0000	0.0009	0.0001	0.001	0.0010	0.0001	

4) Convolution of IESL

TABLE A-V COPT MODEL OF MULTI-LOADS

		P_L			P_{I}^{*}		
C_{P2H} (MW)	$H_{P2H}=0$	$H_{P2H} = 15$ MW	$H_{P2H} = 30$ MW	$H_{P2H}=0$	$H_{P2H} = 15$ MW	$H_{P2H} = 30$ MW	
0	0	0.0	0.0	1.0	1.0	0.5	
10	0	0.0	0.5	1.0	1.0	0.5	
20	0	0.5	0.0	0.5	0.5	0.0	

TABLE A-VI COPM OF IESL

C	$P_{{\scriptscriptstyle IESL}}$						
C_{P2H} (MW)	$H_{P2H} = -30$ MW	$H_{P2H} = -15$ MW	$H_{P2H}=0$	$H_{P2H} = 15$ MW	$H_{P2H} = 30$ MW		
-30	0	0	0	0	0		
-20	0	0	0.32805	0.03645	0		
-10	0	0.32805	0.10935	0.04455	0.00405		
0	0	0.07290	0.04860	0.01260	0.00090		
10	0	0.00090	0.00855	0.00135	0.00005		
20	0	0	0.00045	0.00005	0		

TABLE A-VII CCPM OF IESL

C_{P2H}			$P_{{\it IESL}}$		
(MW)	$H_{P2H} = -30$ MW	$H_{P2H} = -15$ MW	$H_{P2H}=0$	$H_{P2H} = 15$ MW	$H_{P2H} = 30$ MW
-30	1.0000	1.0000	0.59500	$0.10000 \\ (LOLP_h + \\ LOLP_{e\&h})$	0.00500
-20	1.0000	1.0000	0.59500	0.10000	0.00500
-10	0.6355	0.6355	0.23050	0.06355	0.00500
0	0.1495	0.1495	0.07255	0.01495	0.00095
10	0.0145 $(LOLP_e + LOLP_{e\&h})$	0.0145	0.01045	$0.00145 \atop (LOLP_{e\&h})$	0.00005
20	0.0005	0.0005	0.00050	0.00005	0

TABLE A-VIII ADEQUACY INDICES OF IES

Index	Result
$LOLP_{e\&h}$	0.00145
$LOLP_{e}$	0.01305
$LOLP_h$	0.09855
$LOLP_{e\parallel h}$	0.11305
EENS (MWh/year)	1.31×10^{3}
EHNS (MWh/year)	1.38×10^4

5) Initial Computation (First Subpart)

TABLE A-IX COPT MODEL OF EOHL

C_{P2H}	$P_{\it EOHL}$		P_{EOHL}^*		
(MW)	$H_{P2H} = 15 \text{ MW}$	$H_{P2H} = 30 \text{ MW}$	$H_{P2H} = 15 \text{ MW}$	$H_{P2H} = 30 \text{ MW}$	
-30	0	0	0.10000	0.005	
-20	0.03645	0	0.10000	0.005	
-10	0.04455	0.00405	0.06355	0.005	

 $\begin{tabular}{ll} TABLE A-X \\ P_{\it P2H} \begin{tabular}{ll} WITH COP \begin{tabular}{ll} FABLE A-X \\ OF \begin{tabular}{ll} A-X$

	P_{P}	$P_{P2H(1)}$ (COP = 1.5)			$P_{P2H(2)} (COP = 3)$		
C_{P2H} (MW)	$H_{P2H} = -30 \text{ MW}$	$H_{P2H} = -15 \text{ MW}$	$H_{P2H}=0$	$H_{P2H} = -30$ MW	$H_{P2H} = -15 \text{ MW}$	$\begin{array}{c} H_{P2H} = \\ 0 \end{array}$	
0	0	0	0.0025	0	0	0.05	
10	0	0.095	0	0.95	0	0	
20	0.9025	0	0				

C_{P2H} (MW)	$H_{P2H} = -15 \text{ MW}$	$H_{P2H}=0$	$H_{P2H} = 15 \text{ MW}$	$H_{P2H} = 30 \text{ MW}$
-30	0	0	0	0
-20	0	0	0.0000911	0
-10	0	0.003462	0.0001113	0.00001012
0	0.032896	0.004232	0.0003847	0
10	0.040206	0.003655	0	0

6) Convolution Computation (Second Subpart)

TABLE A-XII NUMERICAL RESULTS OF $P_{\it EOHL\&P2H}$

C_{P2H} (MW)	$H_{P2H} = -15 \text{ MW}$	$H_{P2H}=0$	$H_{P2H} = 15 \text{ MW}$	$H_{P2H} = 30 \text{ MW}$
-30	0	0	0	0
-20	0	0	0.0000911	0
-10	0	0.003462	0.0001113	0.00001012
0	0.032896	0.044438	0.0040398	0

7) Modification Computation (Third Subpart)

TABLE A-XIII NUMERICAL RESULTS OF $P_{I\!E\!SL\&P2H}$

C_{P2H} (MW)	$H_{P2H} = -30$ MW	$H_{P2H} = -15$ MW	$H_{P2H}=0$	$H_{P2H} = 15$ MW	$H_{P2H} = 30$ MW
-30	0	0	0	0	0
-20	0	0	0.32805	0.0000911	0
-10	0	0.32805	0.11281	0.0001113	0.0000101
0	0	0.10579	0.09303	0.0166399	0.0009000
10	0	0.00405	0.00855	0.0013500	0.0000500
20	0	0	0.00045	0.0000500	0

TABLE A-XIV NUMERICAL RESULTS OF $P^*_{\mathit{IESL\&P2H}}$

C_{P2H} (MW)	$\begin{array}{c} H_{P2H} = -30 \\ \text{MW} \end{array}$	$H_{P2H} = -15$ MW	$H_{P2H}=0$	$H_{P2H} = 15$ MW	$H_{P2H} = 30$ MW
-30	1.00000	1.00000	0.56210	0.01920	0.00096
-20	1.00000	1.00000	0.56210	0.01920	0.00096
-10	0.67185	0.67185	0.23396	0.01911	0.00096
0	0.23087	0.23087	0.12102	0.01898	0.00095
10	0.01450	0.01450	0.01045	0.00145	0.00005
20	0.00050	0.00050	0.00050	0.00005	0

TABLE A-V ADEQUACY INDICES OF IESL CONSIDERING P2H

Index	Result
$LOLP_{e\&h}$	0.00145
$LOLP_{e h}$	0.03225
$LOLP_h$	0.01775
$LOLP_{e}$	0.01305
EENS (MWh/year)	1.31×10^{3}
EHNS (MWh/year)	2.64×10^{3}

REFERENCES

- X. Chen, M. B. McElroy, and C. Kang, "Integrated energy systems for higher wind penetration in China: formulation, implementation, and impacts," *IEEE Transactions on Power Systems*, vol. 33, no. 2, pp. 1309-1319, Mar. 2018.
- [2] S. Mashayekh, M. Stadler, G. Cardoso et al., "A mixed integer linear programming for optimal DER portfolio, sizing, and placement in multi-energy microgrids," *Applied Energy*, vol. 187, pp. 154-168, Feb. 2017.
- [3] M. Geidl, G. Koeppel, P. Favre-Perrod et al., "Energy hubs for the future," IEEE Power and Energy Magazine, vol. 5, no. 1, pp. 24-30, Dec. 2006
- [4] K. Hemmes, J. L. Zachariah-Wolf, M. Geidl et al., "Towards multi-source multi-product energy systems," *International Journal of Hydrogen Energy*, vol. 32, no. 10-11, pp. 1332-1338, Aug. 2007
- [5] Z. Pan, Q. Guo, and H. Sun, "Interactions of district electricity and heating systems considering time-scale characteristics based on quasisteady multi-energy flow," *Applied Energy*, vol. 167, pp. 230-243, Apr. 2016.
- [6] S. Chen, Z. Wei, G. Sun et al., "Multi-linear probabilistic energy flow analysis of integrated electrical and natural-gas systems," *IEEE Transactions on Power Systems*, vol. 32, no. 3, pp. 1970-1979, May 2017.
 [7] C. Shao, X. Wang, M. Shahidehpour et al., "An MILP-based optimal
- [7] C. Shao, X. Wang, M. Shahidehpour et al., "An MILP-based optimal power flow in multicarrier energy systems," *IEEE Transactions on Sustainable Energy*, vol. 8, no. 1, pp. 239-248, Jul. 2017.
 [8] H. Sun, Q. Guo, B. Zhang et al., "Integrated energy management sys-
- [8] H. Sun, Q. Guo, B. Zhang et al., "Integrated energy management system: concept, design, and demonstration in China," *IEEE Electrification Magazine*, vol. 6, no. 2, pp. 42-50, Jun. 2018.
 [9] W. Gu, J. Wang, S. Lu et al., "Optimal operation for integrated energy
- [9] W. Gu, J. Wang, S. Lu et al., "Optimal operation for integrated energy system considering thermal inertia of district heating network and buildings." Applied Energy, vol. 199, pp. 234-246, May 2017.
- buildings," Applied Energy, vol. 199, pp. 234-246, May 2017.
 [10] F. Kienzle, P. Ahčin, and G. Andersson, "Valuing investments in multi-energy conversion, storage, and demand-side management systems under uncertainty," IEEE Transactions on Sustainable Energy, vol. 2, no. 2, pp. 194-202, Apr. 2011.
- [11] W. Huang, N. Zhang, J. Yang et al., "Optimal configuration planning of multi-energy systems considering distributed renewable energy," *IEEE Transactions on Smart Grid*, vol. 10, no. 2, pp. 1452-1464, Mar. 2019.
- [12] S. M. Miryousefi Aval, A. Ahadi, and H. Hayati, "Adequacy assessment of power systems incorporating building cooling, heating and power plants," *Energy and Buildings*, vol. 105, no. 236-246, Oct. 2015
- [13] G. Koeppel and G. Andersson, "Reliability modeling of multi-carrier energy systems," *Energy*, vol. 34, no. 3, pp. 235-244, Mar. 2009.

- [14] M. H. Shariatkhah, M. R. Haghifam, G. Chicco et al., "Adequacy modeling and evaluation of multi-carrier energy systems to supply energy services from different infrastructures," *Energy*, vol. 109, pp. 1095-1106, Aug. 2016.
- [15] Y. Lei, K. Hou, Y. Wang et al., "A new reliability assessment approach for integrated energy systems: using hierarchical decoupling optimization framework and impact-increment based state enumeration method," Applied Energy, vol. 210, pp. 1237-1250, Sept. 2018.
- [16] S. Zhang, M. Wen, H. Cheng et al., "Reliability evaluation of electricity-heat integrated energy system with heat pump." CSEE Journal of Power & Energy Systems, vol. 4, no. 4, pp. 425-433, Dec. 2018.
- [17] Y. Liu, Y. Su, Y. Xiang et al., "Operational reliability assessment for gas-electric integrated distribution feeders," *IEEE Transactions on Smart Grid*, vol. 10, no. 1, pp. 1091-1100, Jan. 2019.
- [18] J. Chen, Y. Tao, X. Yue et al., "Fast analytical method for reliability evaluation of electricity-gas integrated energy system considering dispatch strategies," Applied Energy, vol. 242, pp. 260-272, Mar. 2019.
- [19] H. Yang, Y. Zhang, Y. Ma et al., "Reliability assessment of integrated energy system considering the uncertainty of natural gas pipeline network system," *IET Generation, Transmission & Distribution*, vol. 13, no. 22, pp. 5033-5041, Nov. 2019.
- [20] M. Bao, Y. Ding, C. Singh et al., "A multi-state model for reliability assessment of integrated gas and power systems utilizing universal generating function techniques," *IEEE Transactions on Smart Grid*, vol. 10, no. 6, pp. 6271-6283, Nov. 2019.
- [21] S. Wang, Y. Ding, C. Ye et al., "Reliability evaluation of integrated electricity-gas system utilizing network equivalent and integrated optimal power flow techniques," *Journal of Modern Power Systems and Clean Energy*, vol. 7, no. 6, pp. 1523-1535, Nov. 2019.
- [22] X. Fu, X. Zhang, Z. Qiao et al., "Estimating the failure probability in an integrated energy system considering correlations among failure patterns," Energy, vol. 178, pp. 656-666, Apr. 2019.
- [23] Y. Cao, W. Wei, L. Chen et al., "Supply inadequacy risk evaluation of stand-alone renewable powered heat-electricity energy systems: a datadriven robust approach," *IEEE Transactions on Industrial Informatics*, vol. 17, no. 3, pp. 1937-1947, Mar. 2021.
- [24] C. Singh, P. Jirutitijaroen, and J. Mitra, Electric Power Grid Reliability Evaluation: Models and Methods, Hoboken: Wiley-IEEE Press, 2018.
- [25] R. N. Allan, *Reliability Evaluation of Power Systems*, New York: Springer Science & Business Media, 2013.
- [26] R. Billinton and Y. Gao, "Multistate wind energy conversion system models for adequacy assessment of generating systems incorporating wind energy," *IEEE Transactions on Energy Conversion*, vol. 23, no. 1, pp. 163-170, Mar. 2008.
- [27] S. Sulaeman, M. Benidris, J. Mitra et al., "A wind farm reliability model considering both wind variability and turbine forced outages," *IEEE Transactions on Sustainable Energy*, vol. 8, no. 2, pp. 629-637, Apr. 2017.
- [28] C. Fan, F. Li, W. Feng *et al.*, "Reliability assessment method of composite power system with wind farms and its application in capacity credit evaluation of wind farms," *Electric Power Systems Research*, vol. 166, pp. 73-82, Oct. 2018.
- [29] X. Zhang, L. Che, M. Shahidehpour et al., "Reliability-based optimal planning of electricity and natural gas interconnections for multiple energy hubs," *IEEE Transactions on Smart Grid*, vol. 8, no. 4, pp. 1658-1667, Jul. 2017.
- [30] C. E. Kim and M. G. Strintzis, "High speed multidimensional convolution," *IEEE Transactions on Pattern Analysis and Machine Intelli*gence, vol. 3, pp. 269-273, May 1980.
- [31] S. Chen, Z. Wei, G. Sun et al., "Adaptive robust day-ahead dispatch for urban energy systems," *IEEE Transactions on Industrial Electron*ics, vol. 66, no. 2, pp. 1379-1390, Feb. 2019.
- [32] M. R. Haghifam and M. Manbachi, "Reliability and availability modelling of combined heat and power (CHP) systems," *International Jour*nal of Electrical Power & Energy Systems, vol. 33, no. 3, pp. 385-393, Mar. 2011.
- [33] N. Zhang, X. Lu, M. B. McElroy et al., "Reducing curtailment of wind electricity in China by employing electric boilers for heat and pumped hydro for energy storage," *Applied Energy*, vol. 184, pp. 987-994, Dec. 2016.

- [34] Y. Jia, P. Wang and X. Han et al., "A fast contingency screening technique for generation system reliability evaluation," *IEEE Transactions on Power Systems*, vol. 28, no. 4, pp. 4127-4133, Nov. 2013.
- [35] N. Zhang, C. Kang, D. S. Kirschen et al., "Rigorous model for evaluating wind power capacity credit," *IET Renewable Power Generation*, vol. 7, no. 5, pp. 504-513, Sept. 2013.
- [36] L. L. Garver, "Effective load carrying capability of generating units," IEEE Transactions on Power Apparatus and Systems, vol. 8, pp. 910-919, Aug. 1966.
- [37] M. Naghizadeh and M. D. Sacchi, "Multidimensional convolution via a 1D convolution algorithm," *The Leading Edge*, vol. 28, no. 11, pp. 1336-1337, Nov. 2009.
- [38] B. Arambepola and P. J. W. Rayner, "Efficient transforms for multidimensional convolutions," *Electronics Letters*, vol. 15, no. 6, pp. 189-190, Feb. 1979.

Chao Yan received the B.E. degree in electrical engineering from Xi'an Jiaotong University, Xi'an, China, in 2010. He is currently pursuing the Ph.D. degree in electrical engineering at the same university. He was a Visiting Scholar at Texas A&M University, College Station, USA, from 2019 to 2020. His research interests include power system risk evaluation, power system planning, and integrated energy system.

Zhaohong Bie received the B.S. and M.S. degrees in electric power from Shandong University, Jinan, China, and the Ph.D. degree from Xi'an Jiaotong University, Xi'an, China, in 1992, 1994, and 1998, respectively. Currently, she is a Professor with the State Key Laboratory of Electrical Insulation and Power Equipment and the School of Electrical Engineering, Xi'an Jiaotong University. Her research interests include power system planning and reliability evaluation, as well as power system resilience.

Shiyu Liu received the B.E. degree from Hohai University, Nanjing, China, in 2014. She is currently pursuing the Ph.D. degree at Xi'an Jiaotong University, Xi'an, China. Her research interests include electricity power market and renewable energy integration.

Dogan Urgun received the B.E. degree in electrical engineering from Erciyes University, Kayseri, Turkey, in 2010, and the M.Sc. degree from Atilim University, Ankara, Turkey, in 2012. He is currently working toward the Ph.D. degree with Texas A&M University, College Station, USA. His research interests include power system optimization, power systems reliability, and artificial intelligence applications for power system and electricity market.

Chanan Singh received the D.Sc. degree from the University of Saskatchewan, Saskatoon, Canada, in 1997. He is currently a Regents Professor and the Irma Runyon Chair Professor with the Department of Electrical and Computer Engineering, Texas A&M University, College Station, USA. He served as the Department Head of Electrical and Computer Engineering Texas A&M from 1997 to 2005 and then as an Interim Head from 2012 to 2015. He also served as a Program Director with the National Science Foundation of USA and a Guest Professor with Tsinghua University, Beijing, China. Dr. Singh is a member of the National Academy of Engineering, Washington DC, USA. He is the recipient of the 1998 Outstanding Power Engineering Educator Award given by the IEEE Power Engineering Society. He was the recipient of the Merit Award by the PMAPS International Society for life long achievements. He was the inaugural recipient of the IEEE-PES Roy Billinton Power System Reliability Award. His research and consulting interests include foundational developments and applications of probabilistic methods for planning and operation of power grid.

Le Xie received the B.E. degree in electrical engineering from Tsinghua University, Beijing, China, in 2004, the M.S. degree in engineering sciences from Harvard University, Cambridge, USA, in 2005, and the Ph.D. degree from Carnegie Mellon University, Pittsburgh, USA, in 2009. He is currently a Professor with the Department of Electrical and Computer Engineering, Texas A&M University, College Station, USA. His research interests include modeling and control of large-scale complex systems, smart grid application with renewable energy resources, and electricity market.